Performance evaluation of a multi-slice CT system[a)]

Cynthia H. McCollough[b)] and Frank E. Zink
Department of Diagnostic Radiology, Mayo Clinic, 200 First Street SW, Rochester, Minnesota 55905

(Received 30 June 1999; accepted for publication 2 September 1999)

Our purpose in this study was to characterize the performance of a recently introduced multi-slice CT scanner (LightSpeed QX/i, Version 1.0, General Electric Medical Systems) in comparison to a single-slice scanner from the same manufacturer (HiSpeed CT/i, Version 4.0). To facilitate this comparison, a refined definition of pitch is introduced which accommodates multi-slice CT systems, yet maintains the existing relationships between pitch, patient dose, and image quality. The following performance parameters were assessed: radiation and slice sensitivity profiles, low-contrast and limiting spatial resolution, image uniformity and noise, CT number and geometric accuracy, and dose. The multi-slice system was tested in axial (1, 2, or 4 images per gantry rotation) and HQ (Pitch = 0.75) and HS (Pitch = 1.5) helical modes. Axial and helical acquisition speed and limiting spatial resolution (0.8-s exposure) were improved on the multi-slice system. Slice sensitivity profiles, image noise, CT number accuracy and uniformity, and low-contrast resolution were similar. In some HS-helical modes, helical artifacts and geometric distortion were more pronounced with a different appearance. Radiation slice profiles and doses were larger on the multi-slice system at all scan widths. For a typical abdomen and pelvis exam, the central and surface body doses for 5-mm helical scans were higher on the multi-slice system by approximately 50%. The increase in surface CTDI values (with respect to the single-slice system) was greatest for the 4×1.25-mm detector configuration (190% for head, 240% for body) and least for the 4×5-mm configuration (53% for head, 76% for body). Preliminary testing of version 1.1 software demonstrated reduced doses on the multi-slice scanner, where the increase in body surface CTDI values (with respect to the single-slice system) was 105% for the 4×1.25-mm detector configuration and 10% for the 4×5-mm configuration. In summary, the axial and HQ-helical modes of the multi-slice system provided excellent image quality and a substantial reduction in exam time and tube loading, although at varying degrees of increased dose relative to the single-slice scanner. [S0094-2405(99)03411-2]

Key words: CT Technology, spiral (helical) CT, multi-slice CT, CT image quality, CT radiation exposure

I. INTRODUCTION

Our purpose in this work was to characterize and compare the performance of a new multi-slice CT scanner (LightSpeed QX/i, Version 1.0, General Electric Medical Systems, Milwaukee, WI) relative to a single-slice CT scanner from the same manufacturer (HiSpeed CT/i, Version 4.0, General Electric Medical Systems). The primary differences in these CT systems are illustrated in Fig. 1. On the multi-slice system, the focal spot-to-isocenter and focal spot-to-detector distances have both been shortened and the number of detector elements along the arc of the detector array has been increased. Most importantly, the multi-slice detector is divided into sixteen 1.25-mm elements along the *z*-axis. The multi-slice system can image 20 mm of patient anatomy (referenced to the isocenter) as opposed to the 10-mm maximum coverage per x-ray exposure (in an axial mode) on the single-slice system.

The sixteen detectors can be configured in four ways, as shown in Fig. 2. Data from one, two, three, or four detectors are combined for each of four outgoing data channels. In axial imaging, the user can choose both the number of images per rotation and the nominal image thickness, as shown in Table I. In contrast to single-slice CT scanners, retrospective reconstruction of thinner or thicker scan widths is possible in the axial acquisition mode.

The detector configuration choices for multi-slice helical imaging are the same as in the multi-slice axial mode, four channels each having a *z*-axis length of 1.25, 2.5, 3.75, or 5 mm, with a total active detector length of 5, 10, 15, or 20 mm, respectively (referenced to the isocenter). For helical scanning, the multi-slice reconstruction algorithm uses data from all four interleaving helical data sets (Fig. 3). The multi-slice helical parameter choices available on the system tested are given in Table II.

In single-slice helical CT, pitch is defined as

$$P=\frac{\text{Table travel per rotation}}{T}, \tag{1}$$

where T equals the nominal scan width (i.e., the scan width specified by the operator, which is approximately equal to

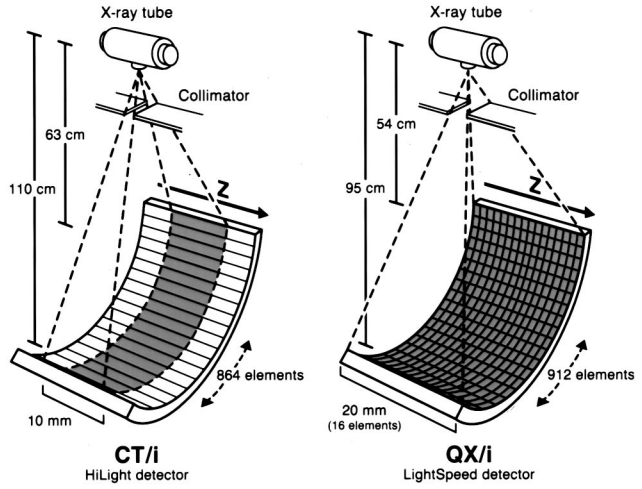

FIG. 1. Illustration of the detectors used in a single-slice (GE HiSpeed CT/i) and multi-slice (GE LightSpeed QX/i) helical CT system. The detector dimensions along the *z*-axis are relative to the isocenter (e.g., the 20-mm depth of the LightSpeed detector is not the actual physical dimension of the detector, but rather the amount of *z*-axis coverage at the isocenter).

the full width at half maximum of the section sensitivity profile) for *one* reconstructed image from the helical volume data set.[1] Although some system designs use post-patient collimation for narrow scan widths or to decrease the contributions of scattered radiation along the *z*-axis, the nominal scan width T is determined primarily by pre-patient collimation (i.e., the width of the incoming x-ray beam along the *z*-axis), as well as the helical interpolation algorithm.

In multi-slice helical CT, where multiple contiguous images can be reconstructed from the data obtained in one gantry rotation, and the nominal scan width is determined primarily by post-patient collimation *and* the helical interpolation algorithm, the concept of helical pitch requires further definition. In recent publications regarding multi-slice helical reconstruction algorithms, Taguchi[2] and Hu[3] use an altered definition of pitch for multi-slice systems:

$$P_{T,H} = \frac{\text{Table travel per rotation}}{t}, \tag{2}$$

where t equals the *z*-axis width of *one* data channel of an N-channel multi-slice detector. The value of t is determined both by the physical size along the *z*-axis of a single detector element and the electronic summation of multiple detector

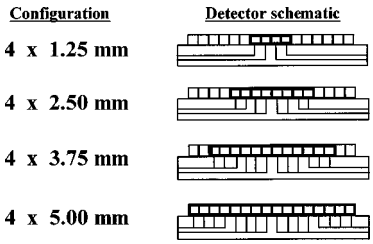

FIG. 2. Illustration of the four detector configurations available on the multi-slice scanner. Four data acquisition channels are used to combine signals from one, two, three, or four individual 1.25-mm detector elements. Once added together, the signal from an individual element cannot be recovered.

TABLE I. Axial imaging modes

	Number of images per rotation		
	4	2	1
Detector configuration	Image thickness (mm)		
4 × 1.25 mm	1.25	2.5	5.0
4 × 2.5 mm	2.5	5.0	10.0
4 × 3.75 mm	3.75	7.5	
4 × 5.0 mm	5.0	10.0	

elements. For example, in the scanner tested, the sixteen 1.25-mm elements are electronically summed to yield t values of 1.25, 2.5, 3.75, or 5 mm.

In single-slice helical CT scanning, a pitch of 1.0 indicates contiguous spacing of the radiation beam spiraling about the patient, which does not alter the dose compared to contiguous axial scanning (assuming the same x-ray technique factors). A pitch of 2.0 causes a gap equal to one x-ray beam width between adjacent spirals, thereby reducing the average patient dose by a factor of two (albeit at the expense of an increase in the width of the section sensitivity profile

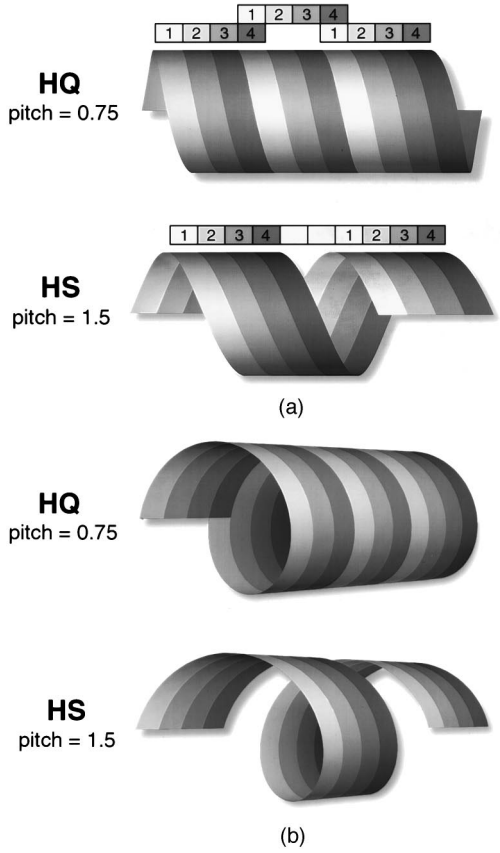

FIG. 3. (a) Side views and (b) oblique views of the helical paths about the isocenter for the HQ and HS modes of data acquisition. The 4 data channels of the total active detector are represented by the four bands of gray. In the HQ mode (pitch = 0.75), the table travel per rotation is equal to the width of 3 data channels, causing the first data-channel path from rotation 2 to overlap the fourth data-channel path of rotation 1. In the HS mode (pitch = 1.5), the table travel per rotation is equal to the width of 6 data channels, causing a gap equal to the width of 2 data channels between the first data-channel path of rotation 2 and the fourth data-channel path of rotation 1.

TABLE II. Acquisition parameters for the HQ (high quality, pitch = 0.75) and HS (high speed, pitch = 1.5) helical imaging modes

Detector configuration	Image thickness (mm)			Table travel (mm per rotation) HQ	HS
4 × 1.25 mm	1.25	2.5		3.75	7.5
4 × 2.5 mm	2.5	3.75	5.0	7.5	15.0
4 × 3.75 mm	3.75[a]	5.0	7.5	11.25	22.5
4 × 5.0 mm	5.0	7.5	10.0	15.0	30.0

[a]3.75-mm thickness not available at 22.5 mm/rotation.

and the severity of helical artifacts). Pitch values less than 1.0 imply overlapping radiation beams and a corresponding increase in average patient dose. To summarize the relationship between dose and pitch under Eq. (1), dose is *inversely* proportional to pitch and a pitch of one yields an equivalent dose compared to contiguous axial scanning (assuming the same x-ray technique factors).

In the context of multi-slice imaging, Eq. (2) is undesirable as it alters the absolute relationship between radiation dose, x-ray beam overlap, and pitch already established in single-slice helical CT [using Eq. (2) for a multi-slice scanner that acquires N simultaneous data channels, a pitch of N indicates contiguous spacing of the radiation beam spiraling about the patient]. In advocating the adoption of Eq. (2) for multi-slice pitch, Hu[3] notes that $P_{T,H}$ ''consistent with the single-slice definition, ... indicates roughly the number of contiguous slices that can be generated over the table translating distance in one gantry rotation.'' However, in the multi-slice environment the number of contiguous images produced per gantry rotation is variable. In the system tested, the number of contiguous slices that can be generated per gantry rotation is dependent upon the prospective (prior to scan acquisition) choice of table speed and detector configuration, as well as the prospective *or* retrospective (before *or* after scan acquisition) choice of reconstructed scan thickness. For example, 1.5, 2, or 3 contiguous slices can be generated per gantry rotation (corresponding to 10-, 7.5-, or 5-mm scan widths) for the 4×5-mm detector configuration and 15 mm per rotation table speed, and 3, 4, or 6 contiguous slices can be generated per gantry rotation (corresponding to 5-, 3.75-, or 2.5-mm scan widths) for the 4×2.5-mm detector configuration and 15 mm per rotation table speed.

In the context of multi-slice imaging, Eq. (1) is inadequate as it fails to account for the ability of the multi-slice reconstruction algorithm to produce images of various nominal scans widths T from a single volume data acquisition (a given table speed and data channel width t, as in the above examples). The density of the helical data (which is the primary determinant of helical image quality[3] and should be reflected by the pitch value) is a function of data channel width t, which does not have a one-to-one correspondence with nominal scan width T.

In order to maintain the established, and intuitive, relationship between helical pitch and radiation dose determined by Eq. (1), and to account for the increased complexity of multi-slice CT, we advocate a *single* definition of pitch, similar to that of Eq. (1), which incorporates an expanded definition of nominal scan width,

$$P' = \frac{\text{Table travel per rotation}}{T'}, \tag{3}$$

where T' equals the *total* nominal scan width along the $z$axis for either a single- or multi-slice system. In single-slice helical CT, the *total nominal scan width* T' along the z-axis remains equal to the nominal scan width T of *one* scan. In multi-slice helical CT, the *total nominal scan width* T' is equal to Nt (the number of active data channels times the z-axis width of a single data channel) and represents the *total active detector width* along the z-axis. [Because of the flexibility of multi-slice helical reconstruction, as demonstrated in the above examples, the *total nominal scan width* cannot be unambiguously determined by the reconstructed (or nominal) scan width, but rather must be determined by the total active detector width.]

With use of our preferred definition of pitch [Eq. (3)], pitch values less than 1.0 alert the user that radiation overlap is occurring and that the dose is increased relative to an axial acquisition with the same technique factors. For an $N = 4$ multi-slice scanner and a 5-mm data channel width, the total active detector width (*total nominal scan width* T') is 20 mm. At a table speed of 15 mm per rotation, the pitch value computed using Eq. (3) is 0.75, which is consistent with a 25% overlap of the radiation beam between consecutive rotations. In the remainder of this manuscript, pitch is computed using Eq. (3).

The need to distinguish between Eqs. (1) and (2) with respect to multi-slice CT was also recognized by Boone *et al.*,[4,5] who referred to Eq. (1) as ''collimator pitch'' and Eq. (2) as ''detector pitch.'' Our preferred definition [Eq. (3)], which is essentially a refinement of the original definition of pitch to accommodate multi-slice systems, provides a *single* definition of ''pitch'' which can be unambiguously applied to both single- and multi-slice systems, avoids the confusion caused by multiple definitions of pitch, and maintains the existing relationships between pitch, patient dose, and image quality.

The multi-slice helical scanner described herein offers users the choice of two pitch values, which the manufacturer terms the high quality (HQ) or high speed (HS) modes of operation. The HQ mode operates at a helical pitch of 0.75 and the HS mode operates at a helical pitch of 1.5. These modes represent two choices of pitch which provide optimized image quality.[2,3] While the choice of multi-slice pitch definition is important for an accurate understanding of the technology and subsequent dose calculations, it can, for the most part, be ignored by users of the system tested. This is because the user interface solely refers to the choice of helical acquisition mode (HQ or HS) and nowhere defines a specific pitch value. This may not be true for multi-slice systems from other manufacturers.

II. MATERIALS AND METHODS

The following image quality and dose performance parameters were assessed using previously described methods:[6–8] low-contrast and limiting spatial resolution, image uniformity and noise, CT number accuracy, slice sensitivity profiles, helical artifacts, radiation dose profiles, and the computed tomography dose index (CTDI). Low-contrast resolution, limiting spatial resolution, and CT number accuracy were assessed with use of a commercially available CT image quality phantom (Catphan 500 with modules CTP401, CTP528, and CTP515, The Phantom Laboratory, Cambridge, NY). Image uniformity and noise were measured with use of a 32-cm diameter cylindrical acrylic shell filled with deionized water. A solid uniformity phantom was also examined (Catphan 500 with module CTP486 and a 30-cm diameter body annulus CTP539). Section sensitivity profiles were measured using the three-dimensional impulse function method and a 0.288-mm tungsten carbide bead (Catphan 500 with module CTP528).[9,10]

Helical artifacts were assessed using two test objects which varied significantly along the *z*-axis: a scan width ramp (Model 463 Economy CT Phantom, RMI Inc., Middleton, WI) and a tungsten wire oriented 23° to the imaging plane (Catphan 500 with module CTP401). Radiation dose profiles were measured with use of a film technique (400–450 mAs at 120 kVp, Kodak X-Omat V, Eastman Kodak Co., Rochester, NY).[11,12] CTDI was measured using previously described techniques,[13–16] 16- and 32-cm diameter CTDI phantoms (head and body, respectively), and a 10-cm long CT pencil ionization chamber and electrometer (model 10×5-10.3 CTDI chamber and MDH model 1015 electrometer, Radcal, Monrovia, CA).

Data were collected on a single-slice (HiSpeed CT/i) and multi-slice (LightSpeed QX/i) CT system from the same manufacturer (General Electric Medical Systems, Milwaukee, WI), both located at our institution. Technique factors were chosen to approximate clinical body CT imaging (120 kVp, 0.8- and 1.0-s exposures, 5- and 10-mm scan widths, and 210 to 410 mA).

III. RESULTS

Low-contrast and limiting spatial resolution, image uniformity and noise, and CT number accuracy were not significantly different on the two systems evaluated. The minimum resolvable diameter of the 0.5% contrast supra-slice test objects (*z*-axis length = 40 mm, CatPhan module CTP515) was approximately 4 to 5 mm on both scanners for the variety of modes tested. Some subtle loss of low-contrast resolution was noted for single-slice helical scans compared to single-slice axial scans at the same technique (280 mAs), as would be expected due to the increased noise of the 180° LI interpolation.[17] On the multi-slice system, when noise was held constant (which required varying the mAs; see Table III), low-contrast resolution (4 to 5 mm at 0.5%) was comparable for 5-mm scans obtained with the various acquisition modes.

TABLE III. Image noise (standard deviation of pixel values, in HU) for nominal 5-mm scans for the single-slice (SS) and multi-slice (MS) scanners.

Scanner	Pitch	Table speed (mm/rotation)	mAs	Noise (HU)[a]
SS	1	5	280	12.1
SS	2	10	280	12.7
MS	(axial)	(4 × 5 mm)	260	11.3
MS	0.75	7.50	210	10.2
MS	0.75	11.25	220	9.9
MS	0.75	15.00	260	9.7
MS	1.5	15.00	400	10.0
MS	1.5	22.50	410	8.9
MS	1.5	30.00	330	9.9

[a]Phantom: CatPhan Module CTP486.

Limiting spatial resolution was about 7 lp/cm using the CatPhan modules and the ''standard'' reconstruction algorithm on both the single-slice and multi-slice systems. A subtle reduction in limiting spatial resolution was noted on the single-slice scanner for scans using a 0.8-s exposure time.

Image uniformity, measured as the edge-to-center difference in mean CT number on the 32-cm diameter water phantom, was also similar between the single-slice and multi-slice scanner. Values ranged from 1.5 to 4.5 HU. Variation in the noise at the periphery of the water phantom was evident on helical scans for both the single-slice and multi-slice scanners, and was approximately 3 to 4 HU. This effect has been previously reported for helical CT.[18]

As expected, image noise was independent of pitch (for the same mAs and scan width) on the single-slice scanner. This was not the case for the multi-slice scanner. The system software automatically adjusts the scan mA as the user alters the acquisition parameters (multi-slice axial, HQ or HS helical, table speed, or scan width) in order to obtain comparable image noise. Using the suggested mAs values, we found image noise to remain relatively constant on the multi-slice scanner as the scan parameters were varied (Table III). Using the 32-cm diameter water phantom, comparable noise ($\approx$ 13.5 HU) was obtained for 5-mm scans using 250 mAs on the single-slice scanner (helical scans, independent of pitch) and 150 mAs on the multi-slice scanner (4×5-mm axial or 5-mm HQ helical scans at a table speed of 15 mm per rotation).

The accuracy and linearity of CT numbers were similar on both scanners. Mean CT numbers for the air, polyethylene, acrylic, and Teflon test objects (nominal values of -1000, 90, 120, and 990 HU, respectively) were −960 to −980 for air, −97 to −86 for polyethylene, 116 to 123 for acrylic, and 999 to 934 for Teflon. A small change in mean CT number (+16 HU for air and −11 to −16 for Teflon) was noted for the 4×3.75-mm and 4×5-mm detector configurations relative to the 4×2.5-mm detector configuration and the single-slice scanner. The slope of the linear fit changed only from 0.96 (single-slice, and multi-slice 4×2.5 and 4×3.75 configurations) to 0.95 (4×5-mm configuration). Mean CT numbers for acrylic were extremely consis-

tent on the multi-slice scanner (121.2 to 123.3) and on the single-slice scanner (116.5 to 117.5). Thus, the small differences in the slope and at the extremes of the CT number range are not likely to be clinically relevant. However, repeated measurements on numerous single-slice and three multi-slice systems have shown consistent results, leading us to believe that these small differences represent true differences between scanner configurations.

The section sensitivity profiles for the single-slice scanner at a pitch of 1.0, 1.5 and 2.0 are shown in Fig. 4(a). The multi-slice scanner sensitivity profiles (HQ and HS modes, table speeds of 7.5 to 30 mm per rotation) are shown in Fig. 4(b). All profiles are for 5.0-mm scans. Table IV details the measured full width at half maximum (FWHM) and full width at tenth maximum (FWTM) values. For table speeds of 7.5 to 15 mm per rotation and 5-mm scans, the section sensitivity profile is actually better than for a single-slice pitch of 1.0. For faster table speeds, 22.5 and 30.0 mm per rotation, the section sensitivity profiles are comparable to a single-slice pitch of 1.5 and significantly better than for a single-slice pitch of 2.0.

More pronounced helical artifacts were noted for the multi-slice scanner from the scan width ramp and wire test objects, which varied significantly along the *z*-axis. The artifacts were not present in the axial acquisition modes. Rather, the multi-slice scanner produced remarkably crisp axial scan width images. With multi-slice helical scanning, spatial distortion of the ramp at higher table speeds was noted. The parallel lines of the scan width ramp began to converge and diverge (Fig. 5). Also, multiple wavelets were noted emanating from the scan width inclined wire (Fig. 6). This artifact has also been reported by Boone.[4] Neither artifact was noted on the single-slice scanner for pitch values up to 2.0.

For single-slice systems, the width of the radiation beam was consistently within 1 mm of the nominal scan width. For the multi-slice system, the radiation beam width significantly exceeded the total scan width (Table V). The CTDI values for the multi-slice system are dependent upon the detector configuration (Table VI). This reflects the differing dose inefficiencies for the various detector configurations, as noted in the radiation dose profile measurements of Table V. The lowest CTDI values were measured when the full *z* extent of the detector was used (4×5-mm configuration) and the highest CTDI values were measured using the 4×1.25-mm configuration.

Measured CTDI values (acquired with a 10-cm ionization chamber) and manufacturer reported CTDI values (which use the FDA-defined integration length of ±7 T) are both reported in Table VI for the single-slice and multi-slice scanners tested. The measured CTDI values for the 4×5-mm configuration of the multi-slice scanner exceed the manufacturer's CTDI values by 12% – 36%, which is most likely due to the difference in the integration length (100 mm versus 70 mm). Published CTDI values were not available for the 4×3.75-, 4×2.5- or 4×1.25-mm configurations. The range of manufacturer reported CTDI values for single-slice scanners using standard head and body techniques are also reported in Table VI.[19] The single-slice scanner studied has CTDI values at the low end of the reported industry values. The multi-slice system studied is at the high end of, or above, the reported industry values for single-slice systems.

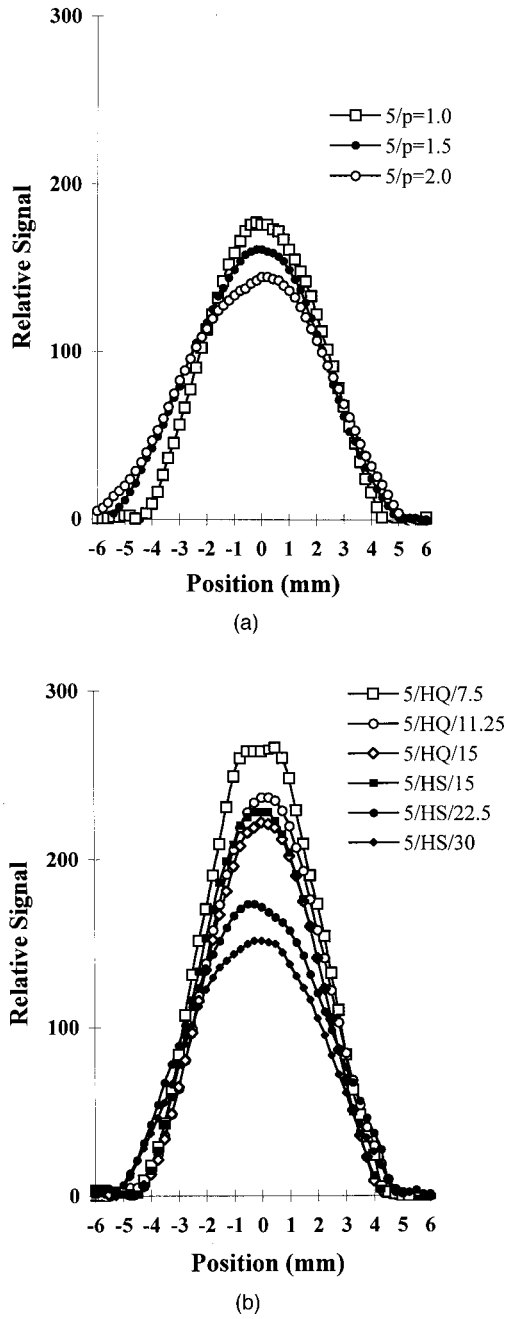

FIG. 4. (a) Single-slice section sensitivity profiles for nominal 5-mm scans. The values in the legend represent the nominal scan width (mm)/pitch. (b) Multi-slice helical section sensitivity profiles for nominal 5-mm scans. The values in the legend represent the nominal scan width (mm)/pitch (HQ =0.75 or HS=1.5)/table speed (mm per rotation).

IV. DISCUSSION

To put the exam acquisition speed, x-ray tube loading, and patient dose differences between the single-slice and multi-slice systems into perspective, we provide a comparison of the acquisition parameters used at our institution for

TABLE IV. Full width at half maximum (FWHM) and full width at tenth maximum (FWTM) of helical section sensitivity profiles for nominal 5-mm scans

Single-slice pitch	FWHM (mm)	FWTM (mm)	Multi-slice mode	Multi-slice mm/rot	FWHM (mm)	FWTM (mm)
1.0	5.1	7.8	HQ	7.5	4.9	7.8
1.5	5.6	9.1		11.25	4.8	7.9
2.0	6.4	10.0		15.0	4.8	7.5
			HS	15.0	4.9	7.6
				22.5	5.9	9.0
				30.0	5.8	9.1

CT examinations of the abdomen and pelvis in Table VII. To image 30 cm of patient anatomy, the single-slice system uses a 7-mm scan width, pitch of 1.0, and requires 34 s. The nominal tube current is 310 mA (250 mAs). The total tube load, represented by the total scan mAs, is about 10,500. The center and surface body CTDI doses were calculated using the *f*-factor for muscle, to better represent patient doses. For the multi-slice system, a 5.0-mm scan width (4×5-mm configuration) in HQ is used. These parameters reduce the scan time to 16 s. Comparable image noise is achieved at 40% less tube current (190 mA or 150 mAs), with a dramatic reduction in overall tube load. Accounting for this mAs reduction and the 25% overlap of the multi-slice spiral (pitch = 0.75), the dose increased approximately 50% at both the center (single-slice: 12 mGy, multi-slice: 18 mGy) and surface (single-slice: 23 mGy, multi-slice: 34 mGy) of a 32-cm CTDI phantom. However, the dose from the multi-slice examination is well within the reported industry range of comparable single-slice examinations.[19]

The multi-slice scanner tested offers a dramatic improvement in acquisition speed with comparable image quality relative to the ''high-end'' single-slice scanner from the same manufacturer. In addition, the multi-slice helical CT reconstruction algorithm produced images with section sensitivity profiles comparable to a pitch of 1.0 to 1.5 for single-slice systems at three to six times the table speed. Some distinctive helical artifacts were noted using high-contrast test objects that varied significantly along the *z*-axis. The presence of four sets of white and dark wavelets (see Fig. 6) suggests that the artifacts are related to the use of four helical data sets (from the four data channels). Clinical evaluations of the multi-slice system are continuing to determine the clinical significance of these artifacts, which occur when a high-contrast object is angled sharply along the *z*-axis. Hence, applications such as CT angiography, skeletal or colon imaging, when performed using the 22.5- and 30-mm per rotation table speeds, may be affected by these artifacts.

In the version 1.0 release of the scanner tested, a significant radiation dose increase was noted relative to single-slice scanners from the same manufacturer. This is due to the dose inefficiency caused by the radiation beam profile being wider than the active detector width. In the multi-slice CT system tested, the radiation beam width must exceed the total active detector width so that the penumbral region does not intersect the outermost detectors (along the *z*-axis) and cause dissimilar section sensitivity profiles amongst the detector arrays. Such differences in section sensitivity profiles would result in image artifacts, since each detector array contributes to the formation of one helical image. The increase in CTDI values (maximum surface values, with respect to the single-slice system) was greatest for the 4×1.25-mm detector configuration (190% for head, 238% for body) and least for the 4×5-mm configuration (53% for head, 76% for body).

According to the manufacturer, the next software release

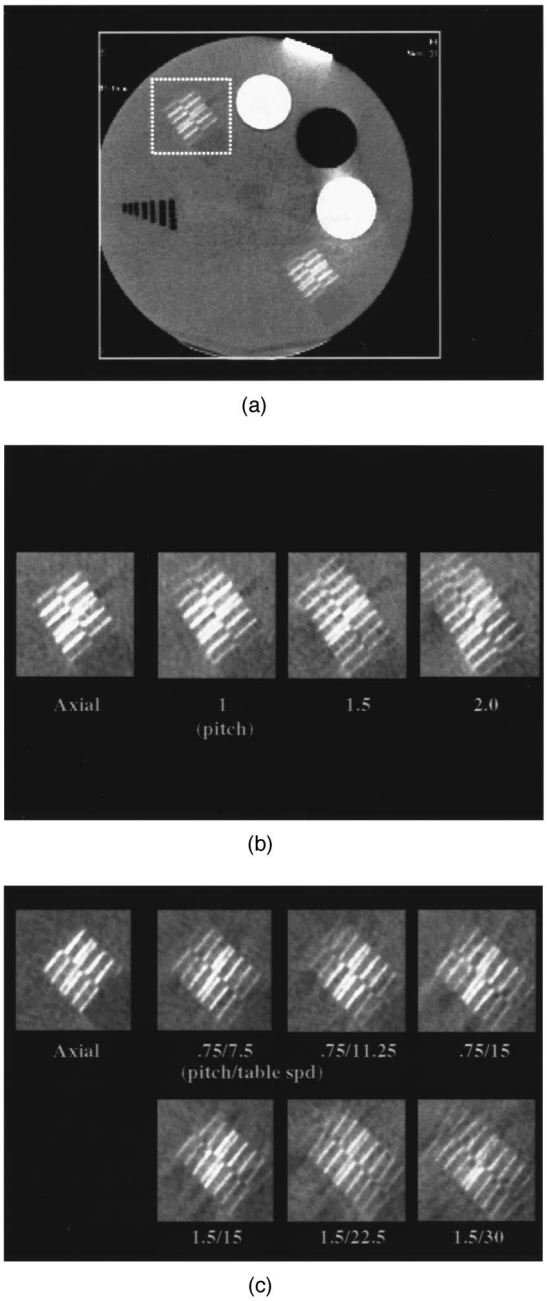

FIG. 5. Demonstration of unique helical artifacts produced on the multi-slice scanner. (a) The complete section of the RMI 423 phantom. The images in (b) single-slice and (c) multi-slice are close-up views of the scan width ramp. The parallel lines within the test object begin to diverge and converge for the multi-slice images as the table speed is increased. This effect was not noted for single-slice pitch values up to 2.0.

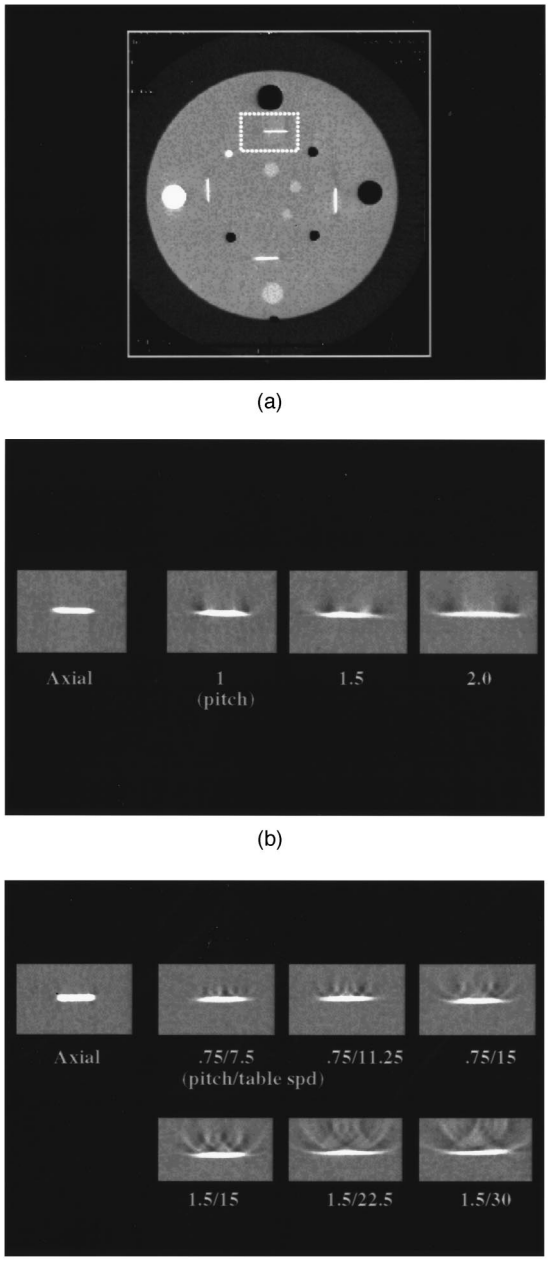

FIG. 6. Demonstration of unique helical artifacts produced on the multi-slice scanner. (a) The complete module CTP401 (Catphan 500 phantom). The images in (b) single-slice and (c) multi-slice are close-up views of the scan width inclined wire. Multiple wavelets are seen emanating from the wire for the multi-slice images as the table speed is increased. This effect was not noted for single-slice pitch values up to 2.0.

(version 1.1) will employ a focal-spot tracking algorithm (software) in conjunction with the existing multi-slice pre-patient collimation system (hardware) to reduce the current dose inefficiencies.[20] We performed body CTDI measurements at the factory using a pre-release version of the focal-spot tracking software. The increase in CTDI values (maximum surface values, with respect to the single-slice system) was still greatest for the 4×1.25-mm detector configuration (105% for body) and least for the 4×5-mm configuration (10% for body). For version 1.1 software, the center body CTDI values in Table VI are reduced from 35, 24, 21, and 19 mGy to 22, 16, 14, and 13 mGy for the 4×1.25, 2.5-, 3.75-, and 5.0-mm configurations, respectively. At the surface, the body CTDI values in Table VI are reduced from 71, 48, 41, and 37 mGy to 43, 31, 24, and 23 mGy for the 4×1.25-, 2.5-, 3.75-, and 5.0-mm configurations, respectively. The overall decrease in the dose inefficiency did not appear to have any detrimental effects on image quality, although we report here only preliminary findings on a factory system. It is important to note the technique factors used in these comparisons (mAs values). The actual difference in patient doses between systems is dependent on the mAs values used in clinical practice.

In conclusion, multi-slice CT is a significant advance in the technology of x-ray computed tomography. Other manufacturers have also announced or will soon be releasing additional multi-slice systems. With this new technology, single-breath-hold, thin-slice volume scanning, without regard to x-ray tube heat limits can be readily accomplished. However, as multi-slice systems are incorporated into many clinical practices, a careful evaluation of all acquisition modes, particularly with regard to radiation dose and helical artifacts, should first be performed and understood in order to appropriately convert existing single-slice clinical protocols, optimize image quality, and minimize patient dose.

TABLE V. Radiation dose profile widths.

Detector configuration	Total nominal scan width	Radiation profile width
4 × 1.25 mm	5 mm	12.5 mm
4 × 2.5 mm	10 mm	16.5 mm
4 × 3.75 mm	15 mm	21.5 mm
4 × 5.0 mm	20 mm	26.0 mm

TABLE VI. Center and Maximum Surface Doses (CTDI, mGy), f-factor = 0.78 (acrylic).

	Measured data					Manufacturer data		
	MS (4 configurations)[a]				SS[a]	MS[b]	SS[c]	Industry range[d]
Total nominal scan width (mm)	5	10	15	20	10	20	10	10
Head - center	117	80	69	62	37	49	40	32–73
Head - surface	116	79	68	61	40	54	40	32–76
Body - center	35	24	21	19	11	14	11	11–20
Body - surface	71	48	41	37	21	33	20	20–42

[a]Measured data: 10-cm CTDI ion chamber, axial scans, 120 kVp, 260 mAs for MS, 340 mAs for SS head, 280 mAs for SS body, with use of ''SmartBeam'' bowtie filter on both systems. These technique factors represent typical clinical parameters at our institution.
[b]LightSpeed QX/i Product Data Sheet (General Electric Medical Systems), 260 mAs, with use of ''SmartBeam'' bowtie filter
[c]HiSpeed CT/i Product Data Sheet (General Electric Medical Systems), 340 mAs, without use of ''SmartBeam'' bowtie filter
[d]Manufacturers' reported data for standard head and body techniques (Ref. 19).

TABLE VII. Abdomen and pelvis clinical exam parameters and dose (0.8 s/rotation, 30-cm coverage, 120 kVp).

	SS-helical	MS-HQ[b]
Scan width/pitch	7/1	5/0.75
Table speed (mm/s)	8.8	18.8
Scan time(s)	34	16
mA	310	190
Total mAs	10,540	3,040
Center dose[a] (CTDI, mGy)	12	18
Max surface dose[a] (CTDI, mGy)	23	34

[a]Measured using a 10-cm CTDI ion chamber and a 32-cm acrylic CTDI phantom, *f*-factor=0.94 (muscle).
[b]Version 1.0 software.

ACKNOWLEDGMENTS

The authors would like to thank Dr. Timothy J. Welch for his assistance in determining optimal clinical exam parameters, and Dr. H. David He and Mr. Sholom Ackelsberg from General Electric Medical Systems for their explanations of the design of General Electric's multi-slice scanner. The authors gratefully acknowledge the expert assistance of Susan R. Miller with regard to manuscript preparation.

[a)]Nothing in this publication implies that the Mayo Foundation endorses the products used in this study.

[b)]Corresponding author and reprint requests: Cynthia H. McCollough, Ph.D., Associate Professor, Department of Diagnostic Radiology, Mayo Clinic, 200 First Street SW, Rochester, Minnesota 55905. Telephone: (507) 284-6875; fax: (507) 284-8996; Electronic mail: mccollough.cynthia @mayo.edu

[1] C. R. Crawford and K. F. King, ''Computed tomography scanning with simultaneous patient translation,'' Med. Phys. **17**, 967–982 (1990).
[2] K. Taguchi and H. Aradate, ''Algorithm for image reconstruction in multi-slice CT,'' Med. Phys. **25**, 550–561 (1998).
[3] H. Hu, ''Multi-slice helical CT: Scan and reconstruction,'' Med. Phys. **26**, 5–18 (1999).
[4] J. M. Boone, ''Computer tomography: Technology update on Multiple Detector Array Scanners and PACS considerations,'' in *Practical Digital Imaging and PACS*, edited by J. A. Seibert, L. J. Filipow, and K. P. Andriole (Medical Physics Publishing, Madison, WI, 1999), AAPM Monograph No. 25, pp. 37–65.
[5] N. M. Corrigan *et al.*, ''A multiple detector array helical x-ray microtomography system for specimen imaging,'' Med. Phys. **26**, 1708–1713 (1999).
[6] C. H. McCollough and F. E. Zink, ''Quality control and acceptance testing of CT systems,'' in *Medical CT & Ultrasound: Current Technology and Applications*, edited by L. W. Goldman and J. B. Fowlkes (Advanced Medical Publishing, Madison, 1995), pp. 437–465.
[7] American Association of Physicists in Medicine, *Specification and Acceptance Testing of Computed Tomography Scanners* (AAPM, New York, 1993), Report No. 39.
[8] L. D. Loo, ''CT acceptance testing,'' in *Specification, Acceptance Testing, and Quality Control of Diagnostic X-Ray Imaging Equipment*, edited by J. A. Siebert, G. T. Barnes, and R. G. Gould (American Institute of Physics, New York, 1994), pp. 863–898.
[9] A. Polacin and W. A. Kalender, ''Measurement of slice sensitivity profiles in spiral CT,'' Med. Phys. **21**, 133–140 (1994).
[10] W. J. Davros *et al.*, ''Determination of spiral CT slice sensitivity profiles using a point response phantom,'' J. Comput. Assist. Tomogr. **19**, 838–843 (1995).
[11] R. L. Dixon and K. E. Ekstrand ''A film dosimetry system for use in computed tomography,'' Radiology **127**, 255–258 (1978).
[12] F. E. Zink and C. H. McCollough, ''The measurement of radiation dose profiles for electron-beam computed tomography using film dosimetry,'' Med. Phys. **21**, 1287–1291 (1994).
[13] T. B. Shope, R. M. Gagne, and G. C. Johnson, ''A method for describing the doses delivered by transmission x-ray computed tomography,'' Med. Phys. **8**, 488–495 (1981).
[14] R. A. Jucius and G. X. Kambic, ''Measurements of computed tomography x-ray fields utilizing the partial volume effect,'' Med. Phys. **7**, 379–382 (1980).
[15] A. Suzuki and M. N. Suzuki, ''Use of a pencil-shaped ionization chamber for measurement of exposure resulting from a computed tomography scan,'' Med. Phys. **5**, 536–539 (1978).
[16] American Association of Physicists in Medicine, *Standardized Methods for Measuring Diagnostic X-Ray Exposures* (AAPM, New York, 1990), Report No. 31.
[17] A. Polacin, W. A. Kalender, and G. Marchal, ''Evaluation of section sensitivity profiles and image noise in spiral CT,'' Radiology **185**, 29–35 (1992).
[18] G. Wang and M. W. Vannier, ''Helical CT image noise—analytical results,'' Med. Phys. **20**, 1635–1640 (1993).
[19] L. N. Rothenberg and K. S. Pentlow, ''CT dosimetry and radiation safety,'' in *Medical CT & Ultrasound: Current Technology and Applications*, edited by L. W. Goldman and J. B. Fowlkes (Advanced Medical Publishing, Madison, 1995), pp. 519–556.
[20] H. David He (personal communication).